



# Edge trimming of C/PPS plates

Petr Masek<sup>1</sup> · Pavel Zeman<sup>1</sup> · Petr Kolar<sup>2</sup> · František Holesovsky<sup>3</sup>

Received: 6 June 2018 / Accepted: 4 October 2018 / Published online: 30 October 2018  
© The Author(s) 2018

## Abstract

A main requirement in the field of polymer composites milling with fibre reinforcement is to machine with high quality in one operation (without delamination or burrs). That requires precise selection of cutting tool geometry and cutting conditions. Fibre-reinforced plastics (FRPs) are difficult-to-machine materials due to high abrasivity, relatively low melting point of polymeric matrices and inclination to delamination or large burr formation. This study investigates the main factors influencing the forces, temperature and surface quality in terms of the cutting conditions through ANOVA testing. Machining during this experiment was performed with a polycrystalline diamond (PCD) end mill. Next, the strongest factor with various double-helix cutting tool geometry was compared. The geometric model of the cutting forces was created based on previous measurements as well as a general empirical model of cutting forces, temperature on the machined surface and average delamination length for C/PPS material.

**Keywords** Composites with thermoplastic matrix · Edge trimming · Machined surface temperature · Delamination · Cutting forces · Cutting tool geometry

## 1 Introduction

Fibre-reinforced plastics (FRPs) are commonly used for their convenient strength-to-weight ratio and possibility to change their mechanical properties in various directions by modifying the composite compound proportion and placement of fibres in the matrix [1]. Thermoplastic composites (FRTCs) are still more widely used in this group of materials. FRTC possesses the flexibility of varying their properties during milling in comparison to more commonly used thermoset composites, including composites with epoxide resin. Thermoplastic matrices are tougher. Their chip formation mechanisms are more similar to metal materials compared to thermoset composites which create small and dust-like chips [2, 3]. The higher

toughness and plasticity of thermoplastic composites decrease their inclination to delamination during workpiece edge trimming [4]. The machining process is limited by the melting point of the matrix and by delamination occurring as a result of cutting force load. Most publications are focused on the machining of C/epoxy that means thermoset matrices. Studies focused solely on thermoplastic matrices are rare.

The quality of the machined surface is the most mentioned aspect of FRP materials. The most discussed quality parameter is the delamination. The delamination is defined as a separation of the neighbouring plies of the composite [5]. The three types of delamination can be observed after milling as was determined in [6]. The second and third types of delamination are described as uncut fibres and matrix partially attached to the machined edge and has an appearance of fuzz. There is no standardised method for evaluation of delamination, but delamination can be quantified by the delamination factor  $F_d$  [7, 8, 9] or  $A_{del}$  [10]. There are many references for evaluation of delamination on thermoset composites [11–15] but no one for thermoplastic composites.

The temperature in cutting zone is a significant factor which affects the quality of the machined surface and tool life. The glass transition temperature  $T_g$  is considered the critical temperature for machining of FRP [4]. A decrease of mechanical properties can be observed for the thermoplastics when the  $T_g$  is reached. Thermoplastic polymers have  $T_g$  much

✉ Petr Masek  
P.Masek@rcmt.cvut.cz

<sup>1</sup> Department of Production Machines and Equipment, Faculty of Mechanical Engineering, Center of Advanced Aerospace Technology, Czech Technical University in Prague, Technická Street 4, 16607 Prague 6, Czech Republic

<sup>2</sup> Research Center of Manufacturing Technology, Czech Technical University in Prague, Prague, Czech Republic

<sup>3</sup> Department of Machining, Process Planning and Metrology, Czech Technical University in Prague, Prague, Czech Republic

lower than the melting point  $T_m$ . Thus, a decrease of mechanical properties can be observed earlier than damage of the machined surface. The study of the thermal phenomenon during milling of FRP materials is focused mainly on the methodology of the temperature measurement. A comprehensive overview in various recently used methods of temperature measurement during machining was made by Davies [16]. Each measuring method had various physical limitations in application for a given design of an experiment. The limitation presents itself during certain usages of a milling cutter, workpiece material or cutting conditions. Using an artificial thermocouple is possible with the cutting tool [17, 18] or with the workpiece [19], but a design intervention in the cutting tool or workpiece is necessary. Thermography is also an applicable measuring method for FRP materials. A pyrometer was used in [20] as the main temperature detector. As an additional measurement device, an infrared camera was utilised in [18, 21]. Nevertheless, the cutting temperature cannot be measured by artificial thermocouple or thermography. Cutting temperature can be defined as the mean temperature between all contact areas on the edge of the cutting tool and the workpiece. The measured temperature is only somewhere near the contact area between the cutting tool and workpiece. Only a method with a chip-tool thermocouple can be used for measuring the cutting temperature during milling of FRP [21]. It is possible to use this method only when either the cutting tool or the workpiece material is electrically conductive. The electric conductivity in a workpiece is ensured by carbon fibres. However, this method is not applicable for diamond-coated or polycrystalline diamond (PCD) tools, which are almost insulants and are commonly used for machining FRP. A semi-artificial thermocouple with workpiece material can be used during milling with diamond cutters. The requirement is only electric conductivity of FRP [22].

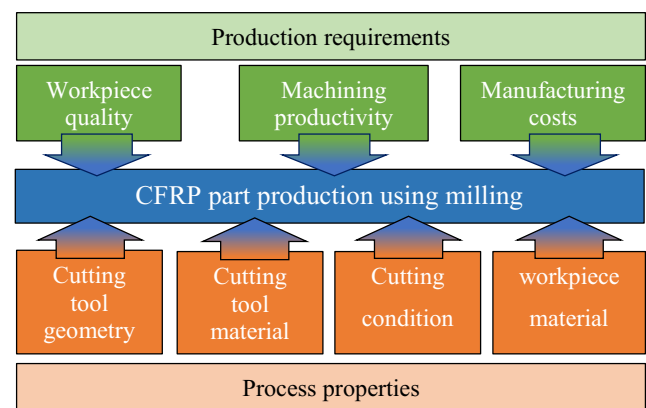
A cutting force is a significant entity which characterises a machining process and can affect the wear of the cutting edge as well as machined surface quality during machining. A magnitude of a cutting force follows on specific cutting force. The coefficients of specific cutting forces for C/PEEK a C/ABS in a different fibre orientation were determined by Puw [23]. Kala utilised neural networks [24] for prediction of the specific cutting force coefficients for C/epoxy. The model for prediction of the cutting forces was determined for a single-helix cutting tool. The relationship between cutting force and fibre orientation in FRP was modelled by Karpát [25]. He also developed a cutting force model for double helix [26]. This type of cutting geometry is mentioned in [27] as suitable for prevention of delamination. Double-helix geometry of a cutting tool was tested in [28, 29]. Opinions on suitability of this geometry vary. However, a double-helix geometry of the cutting tool was recommended to prevent delamination [30].

**Table 1** Properties of C/PPS

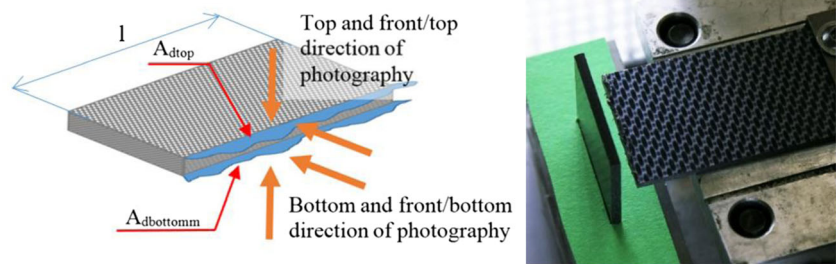
Property	Unit	Value
Ply thickness	mm	0.388
Reinforcement		
Ply orientation	[[[(0.90)/(± 45)]4]s	
Tensile strength	MPa	3530
Elongation	%	1.5
Tensile strength modulus	GPa	230
Density	g/cm <sup>3</sup>	1.76
Electric resistivity	Ω·cm	1.7 × 10 <sup>-3</sup>
Diameter of single fibre	µm	7
Matrix		
Polymer volume in composite	%	50
Glass transition temperature	°C	90
Melting point	°C	258
Chemical resistance		Excellent
Moisture uptake (23 °C, 50% RH)	%	0.03
Thermal conductivity	W/m·°K	0.19
Mechanical properties of composite (bending)		
Ex	MPa	8,751.27
Ey	MPa	36,204.1
Gxy	MPa	874.64

This paper is focused on the edge trimming of thin sheets of polyphenylene sulphide with 4H satin woven carbon fibre T300B reinforcement (C/PPS). It belongs to the semi-crystalline thermoplastic composite family. This type of composite is often used in the aircraft industry, mainly for production of internal panels. Its properties are shown in Table 1.

Monitored values in this study were active cutting force ( $F_a$ ), average delamination length ( $A_{dl}$ ) and temperature of the machined surface ( $\Theta$ ). Values of these entities are affected by both production requirements and process properties (Fig. 1). Suitable methods for measuring the machining

**Fig. 1** Chart of the link between production requirements and properties of workpiece material

**Fig. 2** Principle of the burr measurement (left); arrangement of the specimen during measuring (right)



characteristics are given by the previously stated limitation of the experiment. The C/PPS composite was machined by a diamond-coated sintered carbide tool as well as by a PCD tool in this study. The preferred method of the delamination evaluation is through the average length of the delamination to avoid delamination extremes. That leads to more reliable data for the statistical evaluation. Because carbon fibres in the chosen workpiece material are electrically conductive and the chosen tools are electrically insulated, the semi-artificial thermocouple with C/PPS is a suitable choice for evaluating the machined surface temperature. The preferred procedure for force measuring uses a piezoelectric dynamometer which is sufficiently sensitive and with a high sample rate for measuring small forces during milling operations.

The main aim of this study is to define strong and weak control factors which influence measured  $F_a$ ,  $A_{dl}$  and  $\Theta$  to determinate the model equations. The paper involves three consequential parts:

- Preliminary tests of edge trimming for identification of the most important influence of cutting conditions.
- Investigation of the cutting tool geometry influences the cutting forces, delamination and temperature.
- Mathematical modelling of cutting forces, average length of delamination and temperature of the machined surface for the strongest factor and geometry of the cutting tool.

## 2 Experimental procedure methods

Study of the C/PPS trimming is based on the evaluation of cutting forces, size of the delamination and temperature measured on the machined surface by means of collected data. The method utilised for measuring and evaluating the quantities is described in this section.

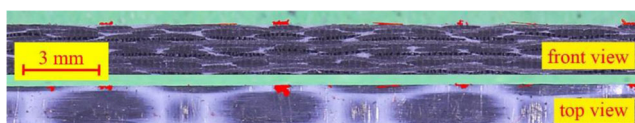


**Fig. 3** Choosing of burr area (red highlight) on the top side of the specimen in the graphic editor

Active force ( $F_a$ ) was calculated from feed force ( $F_f$ ) and normal feed force ( $F_{fN}$ ) (1), which were measured by means of a Kistler 9255B stationary dynamometer. This type of dynamometer was used in preliminary tests because the radial ( $F_c$ ) and tangential ( $F_{cN}$ ) cutting forces were not the objects of the observation. The  $F_a$  was a prior for finding a control factor significance. Moreover, this type of dynamometer gave more accurate results in higher spindle speed regime than the rotating dynamometer.

$$F_a = \sqrt{F_f^2 + F_{fN}^2} = \sqrt{F_c^2 + F_{cN}^2} \quad (1)$$

Tangential ( $F_c$ ) and radial ( $F_{cN}$ ) forces were calculated from torque and tool diameter with knowledge of the dynamometer coordinate system orientation provided by a Kistler 9123C rotating dynamometer. This type of dynamometer was used in the second block of tests. Radial and tangential forces were evaluated to calculate specific radial and tangential cutting forces. This type of dynamometer can measure torque directly. Then the tangential force can be simply expressed based on the tool diameter. Radial force was calculated from the active and cutting force. The measurement by this type of dynamometer was done at low spindle speed.

$A_{dl}$  (2) was evaluated via the graphic-numerical method. A photograph of the machined surface was taken on the top and bottom part of C/PPS as well as the face of the machined surface. A Canon EOS 550D camera was applied with a canon macrolens 100 mm 1:2.8. Complex information was picked up from position measurements of the delamination type II

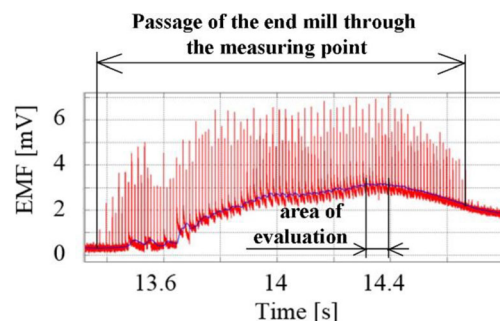
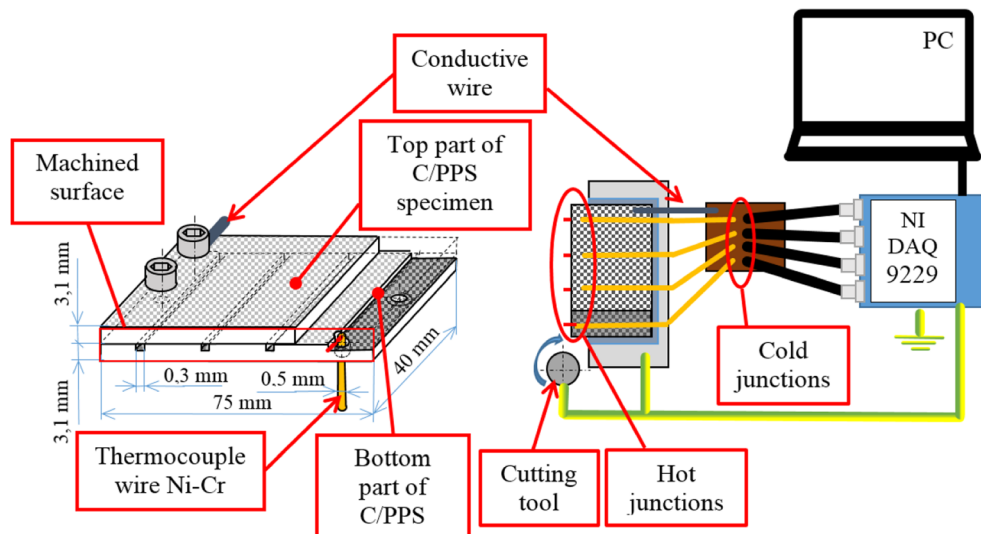


**Fig. 4** A time record of the EMF values by semi-artificial thermocouple Ni–Cr–C/PPS

**Fig. 5** Design of C/PPS specimen (left) and the scheme of semi-artificial thermocouple measuring (right)



or III delamination in the space when two perpendicular directions were photographed in resolution 12,000 pixels per 1 mm<sup>2</sup>. The delamination type II or III occurred only. These two types of delamination include uncut fibres and matrix and make fuzzy appearance. This appearance looks like burr. Therefore, it will be called as “burr” in this article. The entire area of delamination was the sum of the top-edge and the bottom-edge burr on specimen. Proper lighting and contrast control of the background were necessary for correct evaluation of the burr area.

$$A_{dl} = \frac{A_{dtop} + A_{dbottom}}{l} = \frac{\sqrt{(A_t^2 + A_{ft}^2)} + \sqrt{(A_b^2 + A_{fb}^2)}}{l} \tag{2}$$

Here,  $A_{dtop}$  and  $A_{dbottom}$  are areas of delamination (burr) of the top and bottom specimen edge and  $l$  is the machined length (Fig. 2). Next,  $A_t$  is the area of delamination (burr) photographed from the top. Analogically,  $A_b$  is the area photographed in the bottom view. Then  $A_{ft}$  and  $A_{fb}$  are photographed in the face view. Burrs on the edge of the composite were chosen with the help of a graphic editor. The burrs were highlighted; see Fig. 3.

The temperature of the machined surface was measured by means of a semi-artificial thermocouple which utilises electric conductivity of carbon fibres. Nickel–chromium wire was chosen in combination with carbon fibres in the thermocouple. The sensitivity of the thermocouple was 37.6 °C/mV.



**Fig. 6** PCD cutting tool PKD FRAESER 05492-12,000 manufactured by the Gühring company for preliminary tests

Thermocouple calibration was provided under solder with adjustable temperature. The temperature in the hot junction was measured during calibration by the thermocouple type K. Correct function of the semi-artificial thermocouple rests in the defined contact of the Ni–Cr wire and C/PPS. This was ensured by tight imposition of the wire in the laser-machined groove. The laser source with ultrashort pulse duration (a few picoseconds) was used for machining grooves. Minimum affecting of the specimen matrix by heat was achieved. The electric conductivity of the carbon fibres was not changed by laser machining. The fibres are the dominant element for used method of measurement. The wire was, during engagement of the cutter, pushed into the wall of C/PPS groove creating the hot junction. The machined width of grooves was 0.3 mm, the same as the diameter of the wire without any insulation cover. The contact length between C/PPS and Ni–Cr must be small due to occurrence of parasitic thermocouples. They can decrease the real measured electromotive force (EMF). The optimal contact length was found to be in the range from  $a_e + 0.5$  to  $a_e + 1$  mm. The distance between hot and cold junction was 200 mm. This was a sufficient length to avoid heating cold junction with potential influencing of measured EMF.

**Table 2** Parameters of PCD tool

Parameter	Unit	Value
Number of teeth	–	2
Tool diameter	mm	12
Clearance angle	°	10
Rake angle	°	0
Helix angle	°	2.5

**Table 3** DOE—preliminary tests

Parameter/factor	Unit	Symbol	Level	
			1	2
Cutting speed	m/min	$v_c$	100	300
Feed per tooth	mm	$f_t$	0.05	0.1
Radial depth of cut	mm	$a_e$	1	3
Axial depth of cut	mm	$a_p$	3	6

EMF was measured by NI DAQ and the signal was evaluated by the Labview software. The measured signal was filtered by moving average. A higher voltage appeared which repeated in the same frequency as the tooth frequency (Fig. 4). This high voltage represented probably instantaneous deformation of the Ni–Cr wire during machining which was followed by extreme value of temperature. Nevertheless, this temperature was immediately conducted to the surroundings (cutting tool, Ni–Cr wire, C/PPS and air). The various peak of the voltage extreme can be explained with run-out of the cutting edges, run-out of spindle or flatness of uncut surface. The maximum of the temperature of the filtered signal was evaluated as temperature of the machined surface. The scheme of the experimental setup for EMF measurement is presented in Fig. 5.

### 3 Evaluation of cutting conditions factors

These preliminary tests were performed for identification of the most important cutting conditions influencing the cutting forces, machined surface temperature and average delamination length. The results were used for a reduction in the number of the subsequent tests for the main experimental work with investigations for the cemented carbide tools. The milling cutter with PCD cutting edge was used in this preliminary test (Fig. 6 and Table 2). The diameter of the tool was 12 mm. The chosen cutting tool was standard geometry recommended for cutting polymer composites by a well-known producer. This type of cutting tool should offer long tool life with good

quality of a machined surface. A chemical vapour deposition diamond (CVD-diamond) coated compress carbide tool G24L15 (Table 7) was used for comparison of active force in the preliminary test. The design of main block of the experiment will be derived from this comparison.

This tool was set up with precise adjustment of the cutting tool geometry on both cutting edges. The type of cutting material was chosen with regard to durability of the cutting edge to minimise cutting edge wear. The used end mill design was considered “neutral” alternative for the verified double-helix geometry [31]. The main task of the experiment was to measure a significance level of cutting parameters.

The magnitude of the cutting force, delamination factor and temperature of the machined surface during milling were measured. The full factorial design of experiment (DOE) was chosen and the results were evaluated with an ANOVA test. DOE is presented in Table 3. Experiments were performed on the three-axis vertical milling centre with a maximum spindle speed of 15.000 1/min and maximum spindle power of 18 kW. DOE included four control factors  $f_t$ ,  $v_c$ ,  $a_p$  and  $a_e$  (Table 3). The influence of the change of control factors on the active force magnitude, average length of delamination and maximal temperature of the machined surface was investigated.

### 3.1 Results and discussion of preliminary test

An ANOVA test was performed for significance level  $\alpha = 0.05$ . The statistically significant influence of all control factors was proved for  $F_a$ . It can be estimated for PCD tool on the base of the  $F$ -ratio and Tukey’s test that  $F_a$  was the most affected by the control factor  $a_p$  (Table 4, left), then the  $f_t$  and  $a_e$ . According to the main effect plot for mean values, it is obvious that the higher the control factors  $f_t$ ,  $a_p$  and  $a_e$  were, the higher the active force was (Fig. 7, blue). Conversely, if  $v_c$  was increased, then  $F_a$  was decreased. ANOVA does not take into account differences in unit order or units at all. If the guideline coefficients will be compared, the steepest trend can be measured for  $f_t$ . The same situation can be derived for CVD diamond-coated compress tool where the  $a_e$  had

**Table 4** The ANOVA test results for  $F_a$ —PCD tool (left) and CVDD-coated compress tool (right)

Source	DF	Seq SS	Adj SS	Adj MS	F	P	Source	DF	Seq SS	Adj SS	Adj MS	F	P
$a_e$	1	43.9	43.9	43.9	22.9	0	$a_e$	1	4736	4736	4736	36.29	0
$a_p$	1	1422.7	1422.7	1422.7	742.1	0	$a_p$	1	2773	2773	2773	21.25	0.001
$v_c$	1	13.2	13.2	13.2	6.9	0.014	$v_c$	1	9.7	9.7	9.7	0.07	0.79
$f_t$	1	69.2	69.2	69.2	36.1	0	$f_t$	1	640.8	640.8	640.8	4.91	0.049
Error	27	51.8	51.8	1.9			Error	27	1435.4	1435.4	130.5		
Total	31	1600.7					Total	31	9595				

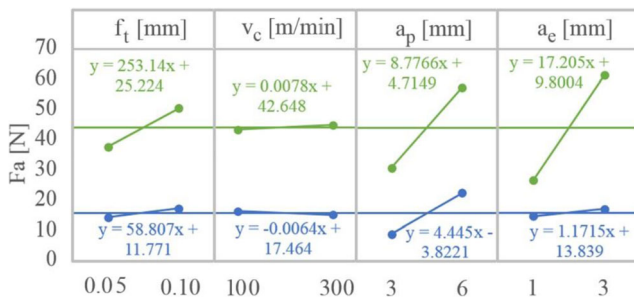


Fig. 7 Main effect plot for mean values of  $F_a$ –PCD tool (blue) CVD diamond-coated compress tool (green)

the strongest significance because of more teeth in engagement at once, but the steepest trend had also the control factor  $f_t$ . This factor was close to reject the zero hypothesis for CVD diamond-coated tool in the ANOVA results, but still statistically significant on the signification level  $\alpha = 0.05$  (Table 4, right). The cutting speed was calculated as insignificant for CVD diamond-coated tool.

Evaluation of the  $A_{dl}$  shows the statistical significance of all control factors again. According to  $F$ -ratio and Tukey’s test, it is possible to determine  $a_p$  as the most significant (Table 5).  $A_{dl}$  decreased with increased  $a_p$ . It can be explained by variform geometry along the length of the cutting edge, due to the slope of a cutting edge, the rake angle increases from the point to the end of the cutting edge. A higher rake angle could cause the significant reduction of the  $A_{dl}$ . The second most significant control factor was similarly observed in measuring  $F_a$ , feed per tooth and then the axial depth of cut.  $A_{dl}$  decreased with  $f_t$  and increased with  $a_e$ . When  $v_c$  was increasing,  $A_{dl}$  was decreasing Fig. 8.

In the case of the temperature measurement, the zero hypothesis was not cancelled on the significance level of 5% for control factor  $v_c$  only. The other control factors were statistically insignificant (Table 6). On the basis of the  $F$ -ratio, the  $f_t$  was more false-significant than the  $a_p$ . The less false-significant factor was factor  $a_e$ . The higher  $v_c$ ,  $a_p$  and  $a_e$  were, the higher machined surface temperature went, but when  $f_t$  increased, the temperature fell (Fig. 10). The measured temperature was higher than  $T_g$  for PPS matrix for all cutting conditions but still lower than the melting point of the PPS.

Table 5 The ANOVA test results for  $A_{dl}$

Source	DF	Seq SS	Adj SS	Adj MS	F	P
$a_e$	1	1.208	1.208	1.208	17.03	0.002
$a_p$	1	5.947	5.947	5.947	83.8	0
$v_c$	1	0.352	0.352	0.352	4.97	0.048
$f_t$	1	1.332	1.332	1.332	18.78	0.001
Error	11	0.780	0.780	0.071		
Total	15	9.622				

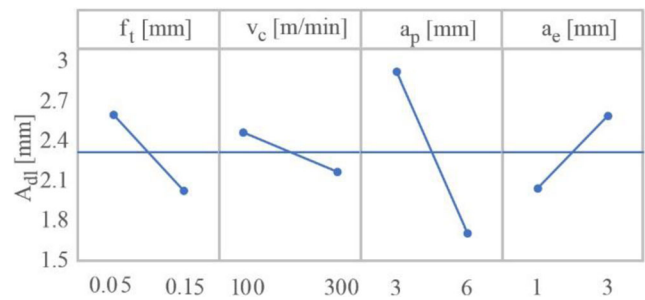


Fig. 8 Main effect plot for means of  $A_{dl}$

Detailed observation of the chips confirmed that there was no heat damage in the chips during a machining process in the whole range of used cutting speeds (Fig. 9). The comparison shows that the structure and shape of the chip were the same at various cutting speeds. The increase of temperature with cutting speed was relatively small, only 18% when cutting speed was tripled (Fig. 10).

On the basis of preliminary experiment results, the most influential factors were chosen for the main block of experimental work. This work was focused on the dependence of cutting tool geometry on cutting forces, burr creation and machined surface temperature. Although  $a_p$  was the most influential factor for  $F_a$  and  $A_{dl}$ ,  $f_t$  was chosen for the next experimental block. If it is considered in the range of the values in tests, steeper dependence is possible to measure in the case of  $F_a$  and  $A_{dl}$  for  $f_t$ . The comparison between PCD- and CVD diamond-coated tools gives the same result in the case of the dependence of  $f_t$  on  $F_a$ .  $f_t$  is the strongest control factor when comparing guideline functions of  $F_a$  dependence on each control factor.  $v_c$  was chosen as the main factor for the second block in the cases of temperature investigation.

### 4 Influence of cutting edge geometry vs. cutting conditions

Mathematical models for cutting forces, average delamination length and temperature are included in the variables of cutting geometry of proper cutting tool type. A double-helix geometry ground in fine cemented carbide and CVD diamond-coated

Table 6 The ANOVA test results for  $\Theta$

Source	DF	Seq SS	Adj SS	Adj MS	F	P
$a_e$	1	194.1	194.1	194.1	1.67	0.222
$a_p$	1	400.8	400.8	400.8	3.46	0.09
$v_c$	1	2282.2	2282.2	2282.2	19.69	0.001
$f_t$	1	529.6	529.6	529.6	4.57	0.056
Error	11	1275.1	1275.1	115.9		
Total	15	4681.8				

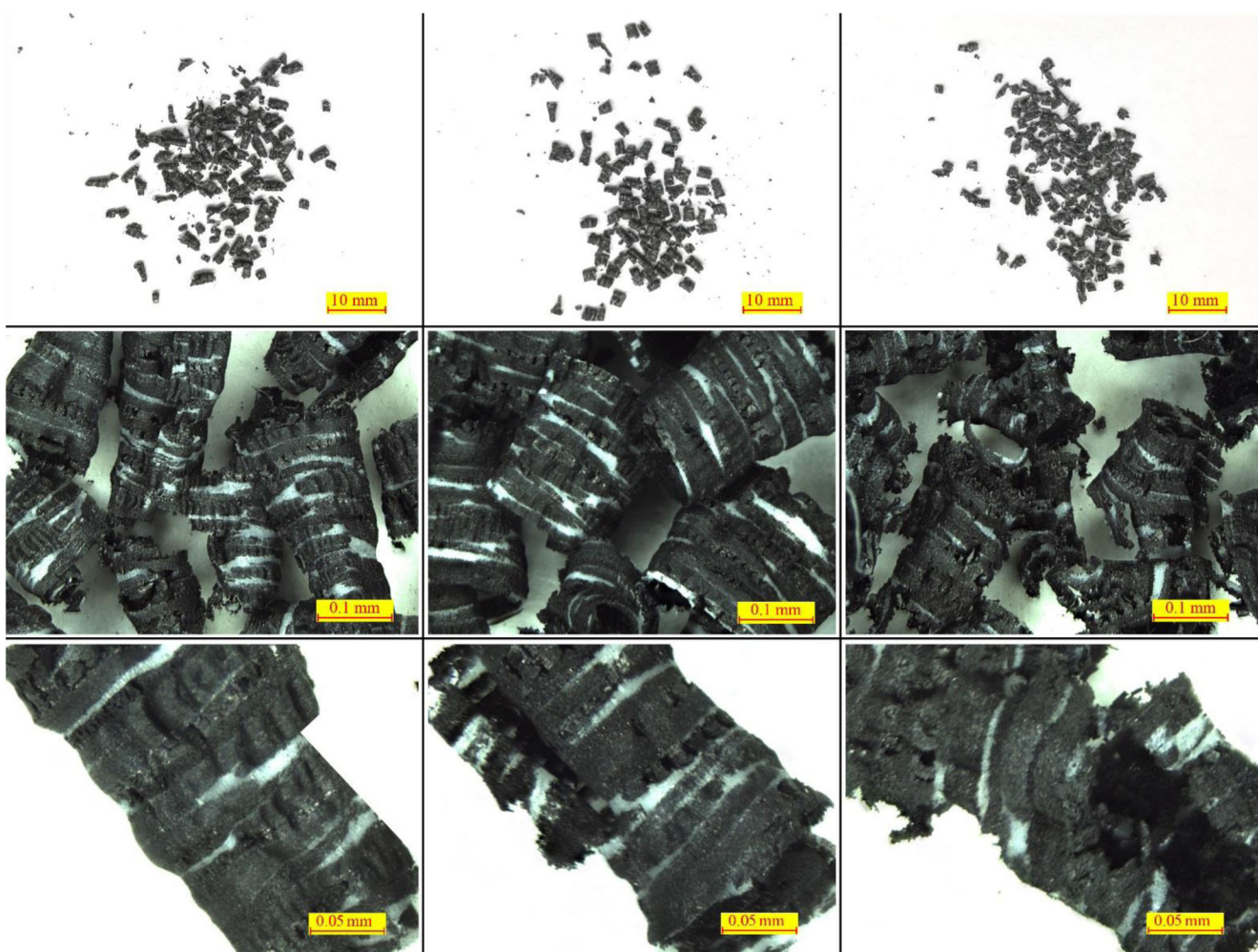


Fig. 9 Comparison of chips collected for different cutting speeds.  $v_c = 100$  m/min (left),  $v_c = 300$  m/min (middle),  $v_c = 500$  m/min (right)

was used in this part of study. A double-helix geometry is more suitable for the machining of FRTC materials. The assumption based on previous experience was that the strongest control factor is the same for PCD- and CVD diamond-coated tools, no matter the tool properties, as was discussed in the previous text. Only CVD diamond-coated tools were used in this block of

$f_i$	1	529.6	529.6	529.6	4.57	0.056
<b>Error</b>	11	1275.1	1275.1	115.9		
<b>Total</b>	15	4681.8				

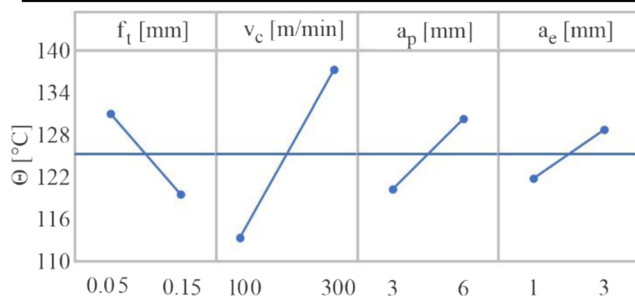


Fig. 10 Main effect plot for means of  $\theta$







experiments. This combination of cutting geometry and cutting tool material minimised delamination and cutting forces [30]. A combination of fine-grained cemented carbide with CVD diamond offers simple adjusting of geometry and relatively long tool life in the cut. Cutting tool parameters are described in Table 7.

Six levels were chosen for factor  $f_i$  and five levels for  $v_c$  (Table 8). The speed limit of the spindle was almost reached in the case of the control factor  $v_c$  at the highest level. The experiment was randomised to avoid time-dependent errors, such as with cutting tool wear.

#### 4.1 Results and discussion of the second block of experiment

Results of the ANOVA test for  $F_a$  show that the control factor rake angle had indemonstrable significance on the chosen significance level. Zero hypothesis had been cancelled for the control factors  $f_i$  and  $\lambda_s$ . These two factors are statistically relevant. Feed per tooth had the highest significance as can

**Table 7** End mills for the second part of experiments

	unit	G25L28	G25L15	G25L5	G15L28	G15L15	G15L5
The view on the cutting part of end mill							
No. of teeth	-				5		
Clearance angle	°				12		
Rake angle	°		25			15	
Helix angle	°	28	15	5	28	15	5

be deduced from results of  $F$ -ratio (Table 9). This was also proven in main effect plots for the mean values of  $F_a$ . The plots show that the higher the rake angle was, the lower  $F_a$  was. Inflexion point in the  $F_a$ - $\lambda_s$  dependence was on the value of  $\lambda_s = 15^\circ$ . The  $F_a$  was the smallest here, but still the trend can be determined as slightly decreasing. Increasing of  $F_a$  after inflexion point can be explained by the mechanism of chip formation. Chips could be pressed to the middle part of compress geometry when higher angles of helix are chosen.  $F_a$  had a rising tendency with  $f_t$  in agreement with preliminary testing (Fig. 11).

It was impossible to cancel alternative hypotheses for all control factors on the basis of  $p$  value in the case of  $A_{dl}$ . All control factors were statistically significant. It was deduced from the results of the  $F$ -ratio that the most significant factor was  $\lambda_s$  and then  $f_t$ . The less statistically significant was  $\gamma_o$  on the size of the burr (Table 10). According to main effect plots, the  $A_{dl}$  decreased with increasing  $f_t$ . The increase followed the power function with high confidence. A higher rake angle can likewise reduce burrs. The helix angle reduces burrs although the ratio of burr reduction was decreasing with helix angle (Fig. 12).

The ANOVA test results for temperature of the machined surface show two statistically significant control factors  $\lambda_s$  and  $v_c$ . Factor  $\gamma_o$  was on the basis of the  $p$  value found to be insignificant.  $F$ -ratio proved that the cutting speed is more significant than  $\lambda_s$  (Table 11). The temperature increased with increasing  $v_c$  according to an exponential function. The temperature decreased with  $\lambda_s$  and slightly increased with  $\gamma_o$  (Fig. 13). The results of  $\gamma_o$  were in accordance with the results from the work of Saglam [32]. The temperature of the machined surface was slightly higher than  $T_g$  for all measurements.

### 5 Geometrical model of cutting forces

The geometrical model of cutting forces follows the Karpát model [26]. Improvement of this model consists in including overlap of the right and left helix marked as  $k$ . This feature avoids uncut fibres and matrix in the middle of the workpiece thickness due to occasional incorrectness in grinding of the tool geometry. This causes the increase in cutting forces due to elongation of both helixes. The overlap can vary from a few tenth of millimetre to several millimetres. A cutting tool was divided to three sections in the

**Table 8** DOE for the second part of experiment

Parameter/factor	Unit	Symbol	Levels					
			1	2	3	4	5	6
Significant factor for $F_a$ and $A_{dl}$	mm	$f_t$	0.03	0.05	0.07	0.1	0.13	0.15
Significant factor for $\Theta$	m/min	$v_c$	100	200	300	400	500	
Rake angle	°	$\gamma_o$	15	25				
Helix angle	°	$\lambda_s$	5	15	28			
Radial depth of cut	mm	$a_e$	3					
Axial depth of cut	mm	$a_p$	3					



**Table 9** The ANOVA test results— $F_a$  vs. geometry and feed per tooth

Source	DF	Seq SS	Adj SS	Adj MS	F	P
$\lambda_s$	2	227.7	227.65	113.82	9.44	0.001
$\gamma_o$	1	40.5	40.51	40.51	3.36	0.078
$f_t$	5	6080.8	6080.78	1216.16	100.9	0
Error	27	325.4	325.44	12.05		
Total	35	6674.4				

model—the left helix, the right helix and the overlap. They are distinguished in the model by axial depth of cut ( $a_{p1}$ ,  $a_{p2}$ ,  $a_{p3}$ ). Each of them engages into material in different time delay  $\psi$ . These three components were summarised in the final calculation.

$$a_{p1} = \begin{cases} 0 & p > m - \frac{k}{2} + a_p \\ a_p & m - \frac{k}{2} - p + a_p > a_p \\ m - \frac{k}{2} - p + a_p & \text{elsewhere} \end{cases} \quad (3)$$

$$a_{p2} = a_p - a_{p1} - a_{p3} \quad (4)$$

$$a_{p3} = \begin{cases} 0 & p < m + \frac{k}{2} \\ a_p & p - m - \frac{k}{2} > a_p \\ p - m - k/2 & \text{elsewhere} \end{cases} \quad (5)$$

A distance from the top of the cutting part of the cutter is  $p$  (mm);  $m$  (mm) is the distance of the middle of the overlap from the end of the cutting part of the cutter. Axial depth of the cut of the right helix in the engage is  $a_{p1}$ , axial depth of the cut of the left helix is  $a_{p3}$  and axial depth of the cut of the overlap is  $a_{p2}$  (Fig. 14).

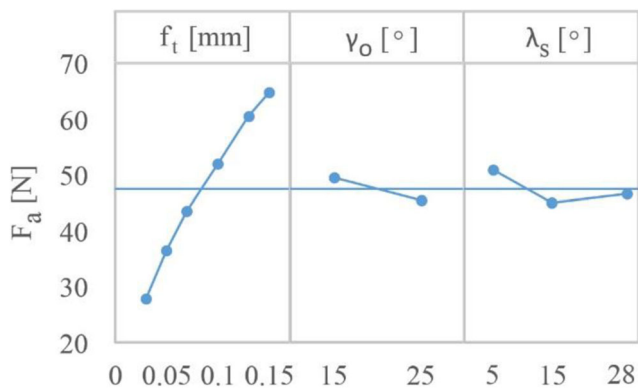


**Fig. 11** Main effect plot for means  $F_a$ —tool geometry vs.  $f_t$ .

**Table 10** The ANOVA test results— $A_{dl}$  vs. geometry and feed per tooth

Source	DF	Seq SS	Adj SS	Adj MS	F	P
$\lambda_s$	2	0.074	0.074	0.037	31.3	0
$\gamma_o$	1	0.0096	0.0096	0.0096	8.09	0.008
$f_t$	5	0.0311	0.0311	0.0062	5.24	0.002
Error	27	0.033	0.033	0.0011		
Total	35	0.1472				

If the position of the cutting tool towards the workpiece is in the axial direction, the width of cut is given by the next rule:

$$b(\varphi) = \begin{cases} \frac{\pi D(\varphi_i - \phi_{st})}{360 \sin \lambda_s} & \phi_{st} \leq \varphi_i \leq \phi_{st} + \tau \\ \frac{\pi D(\phi_{ex} - \varphi_i)}{360 \sin \lambda_s} & \phi_{ex} - \tau \leq \varphi_i \leq \phi_{ex} \\ \frac{a_{pi}}{\cos \lambda_s} & \phi_{st} < \varphi_i < \phi_{ex} \\ 0 & \text{elsewhere} \end{cases} \quad (6)$$

Here, the  $a_{pi}$  generally describes various helixes on the cutting tool. The left helix engages into the cut with the delay  $\psi + \frac{\psi}{2}$ . A delay in the middle part of the cutting tool is defined as  $\psi + \frac{\psi}{2} + \tau$ . Here,  $\tau$  is the additional delay implied from geometrical characteristics on the cutting tool, namely the helix and the overlap. The angle  $\varphi_i$  is instantaneous angle of immersion. The angle  $\phi_{st}$  is the start of immersion and the angle  $\phi_{ex}$  is the end of immersion.

$$\tau = \frac{180(a_p - k) \tan \lambda_s}{\pi D} \quad (7)$$

$D$  is the diameter of the cutting tool. Instantaneous uncut chip thickness is:

$$h(\varphi) = -f_t \frac{\cos \phi_{st} - \cos \phi_{ex}}{\phi_{st} - \phi_{ex}} \quad (8)$$

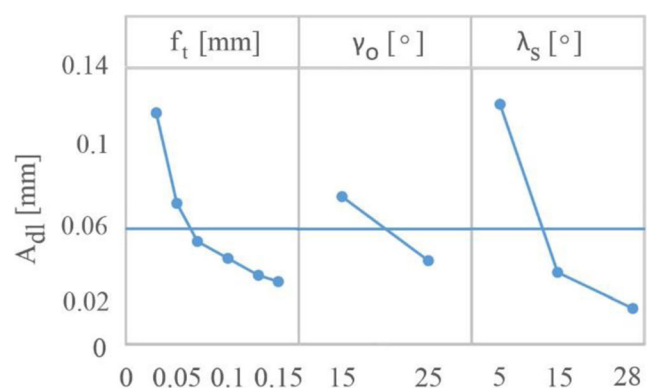


**Fig. 12** Main effect plot for means  $A_{dl}$ —tool geometry vs.  $f_t$ .

**Table 11** The ANOVA test results— $\Theta$  vs. geometry and cutting velocity

Source	DF	Seq SS	Adj SS	Adj MS	F	P
$v_c$	4	3935.6	3935.6	983.9	8.94	0
$\lambda_s$	2	1669.2	1669.2	834.6	7.59	0.003
$\gamma_o$	1	369.1	369.1	369.1	3.36	0.081
Error	22	2420	2420	109.6		
Total	29	8394				

Instantaneous uncut chip thickness for the middle part with the overlap of the cutting edges can be calculated as:

$$h(\varphi) = -\frac{1}{2}f_t \frac{\cos\phi_{st} - \cos\phi_{ex}}{\phi_{st} - \phi_{ex}} \quad (9)$$

The model was based on the assumption of Kienzle’s equation for calculation of the specific cutting force ( $K_c$ ):

$$K_c(\varphi) = kc_1 h(\varphi)^{-m_c} \quad (10)$$

where  $kc_1$  and  $m_c$  are the coefficients of the specific cutting force. Similarly, the specific normal cutting force ( $K_{cN}$ ) can be expressed as:

$$K_{cN}(\varphi) = kc_{N1} h(\varphi)^{-m_{cN}} \quad (11)$$

Here,  $kc_{N1}$  and  $m_{cN}$  are the coefficients of the specific cutting force. Then the cutting (tangential) force is calculated from (12):

$$F_c(\varphi) = K_c(\varphi) \cdot h(\varphi) \cdot b(\varphi) + F_{ce} \quad (12)$$

Normal cutting (radial) force is derived from (11) and (12):

$$F_{cN}(\varphi) = K_{cN}(\varphi) \cdot F_c \quad (13)$$

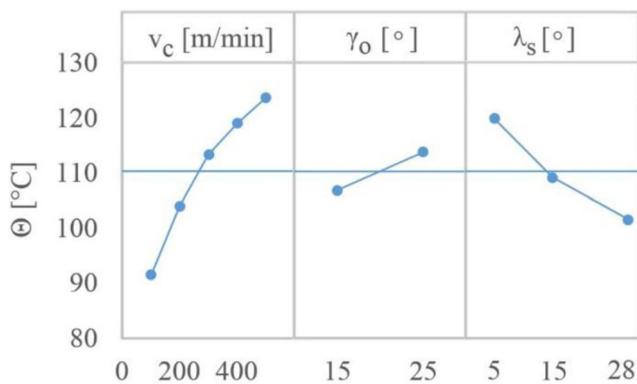


**Fig. 13** Main effect plot for means  $\Theta$ —tool geometry vs.  $v_c$

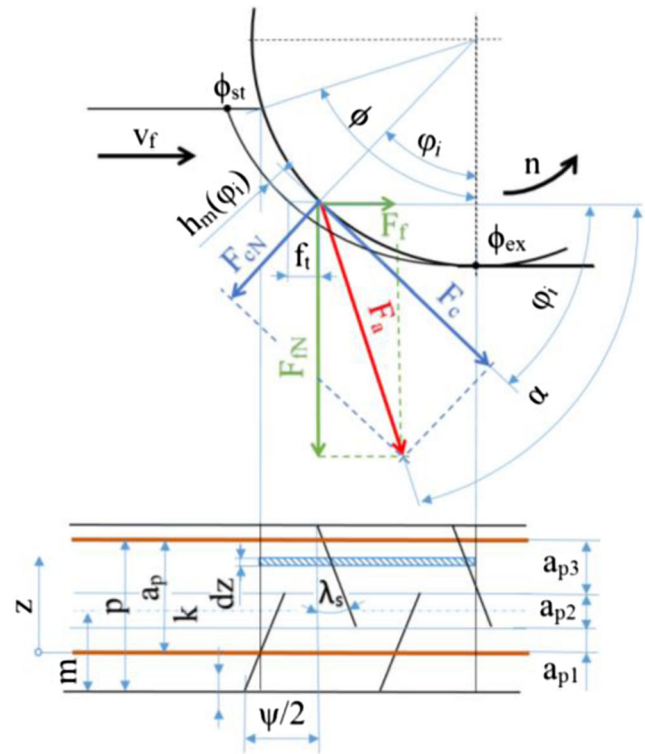


**Fig. 14** Engagement characteristics necessary for model

And then the transformation of  $F_c$  and  $F_{cN}$  to the coordinate system of the dynamometer ( $F_x$  and  $F_y$ ) is possible according to (14) and (15) for comparison of model with measured data.

$$F_x(\varphi) = -F_c(\varphi) \cdot \sin\varphi_i + F_{cN}(\varphi) \cdot \cos\varphi_i \quad (14)$$

$$F_y(\varphi) = F_c(\varphi) \cdot \sin\varphi_i + F_{cN}(\varphi) \cdot \cos\varphi_i \quad (15)$$

**5.1 Verification of cutting force model**

A verification was done for the cutting force model developed with coefficients  $kc_1$ ,  $m_c$ ,  $kc_{1N}$ ,  $m_{cN}$  and  $F_{ce}$  and  $F_{cNe}$ , which were related to the each tested cutting tool. Average error of the model was 3.2%. It was proved that the mathematical model for cutting tools with double helix without including the overlap returns significant differences in results. The difference is affected by the size of  $k$ ,  $\lambda_s$  and  $a_p$ . An influence of  $k$  is decreased by increasing  $a_p$  and decreasing  $\lambda_s$ . An example of the overlap influence is presented in Fig. 15.

**5.2 Generalisation of cutting force model**

It was necessary to find coefficients which include geometrical features of cutters for generalisation of the model. Coefficients for the general cutting force model were obtained from the nonlinear estimate with the least squares method. On

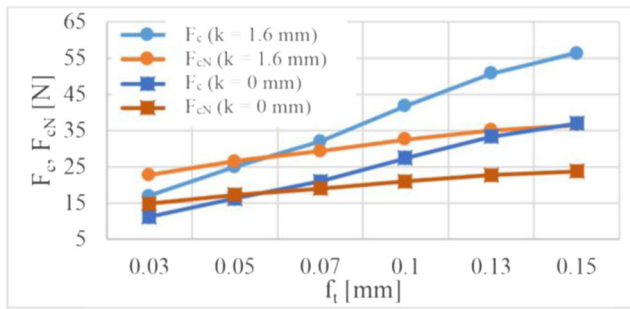


**Fig. 15** Comparison of the modelled relations  $F_c$ - $f_i$  and  $F_{cN}$ - $f_i$  for the cutting tool G25L28 for  $k = 1.6$  mm and  $k = 0$ .  $a_p = 3$  mm

the basis of statistical significance of the chosen coefficients, we found that the coefficients  $m_\gamma$  for the rake angle and  $m_k$  for the overlap were sufficient for reaching the highest accuracy of the model (see Table 12). The final general model for cutting force is described by Eq. (16).

$$F_c(\varphi) = K_c(\varphi) \cdot h(\varphi) \cdot b(\varphi) \cdot \gamma^{-m_\gamma} \cdot k^{-m_k} \quad (16)$$

The regression coefficient for the estimated model was  $R^2 = 0.989$ . The average deviation of all comparison measurements between real and modelled values was 4% and maximum deviation was 15.9%. Comparison of the measured and modelled relationship between  $F_c$  and  $f_i$  for the cutting tools G25L28 and G15L5 is shown in Fig. 16. These two cutting tools were chosen due to verification of cutting force model which was recalculated for  $F_x$  and  $F_y$  (coordinate system of rotary dynamometer) and the real measured force record is presented in Fig. 17. The significant peak errors between model and measured data are probably caused by the dynamic effects between machine tool, cutting tool, measuring device and workpiece. It must be mentioned that rough measuring data without any filtration were used for comparison with cutting model and this could add some differences between measurement and model. Nevertheless, the course and mean values of forces were predicted accurately.

### 5.3 Identification of the delamination model

An empirical model of average delamination length fits the real situation with the highest accuracy by means of Eq. (17).

**Table 12** Estimation of parameters for cutting force model

Table	Estimate parameter	St. dev.	t-value	p value
$k_{c1}$	82.897	6.768	12.248	0.00
$m_c$	-0.265	0.016	-16.385	0.00
$m_\gamma$	-0.201	0.0098	-20.415	0.00
$m_k$	-0.139	0.0253	-5.4851	0.00

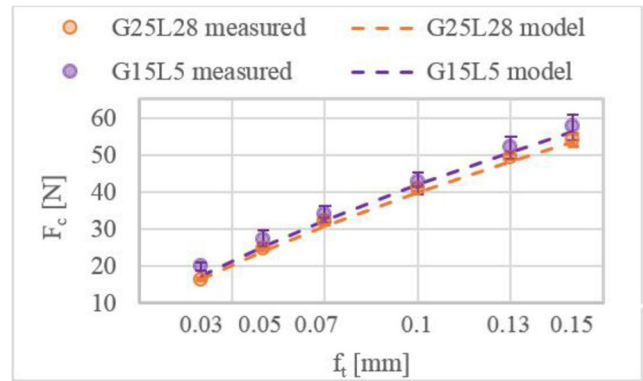


**Fig. 16** Dependence of  $F_c$  model on  $f_i$  compared with measured values for tools G25L28 and G15L5

The dependence  $A_{dl} = f(f_i)$  was estimated in the power course (Fig. 18).

$$A_{dl} = C_{Adl} \cdot f_i^{-uA} \cdot \lambda^{-uA\lambda} \cdot \gamma^{-uA\gamma} \quad (17)$$

The coefficient  $C_{Adl}$  showed considerable high  $p$  value. This indicates a small statistical significance of this coefficient as Table 13. This small statistical significance was not taken into account because without this coefficient, other versions of the model had a substantially smaller regression coefficient. Regression coefficient of the estimated model was  $R^2 = 0.966$ . The average deviation of the delamination model from the real measurement was 37%. However, the maximum deviation from the model was very high, almost 191%. There was a strong deviation in the respective measurement of  $A_{dl}$ . The creation of delamination is almost unpredictable phenomenon. Nevertheless, with higher amount of repetition of experiment and very strong influencing factor, as  $f_i$  was, presented power dependence can be estimated presented. The big deviances in measured  $A_{dl}$  below  $f_i = 0.06$  mm can be explained by small

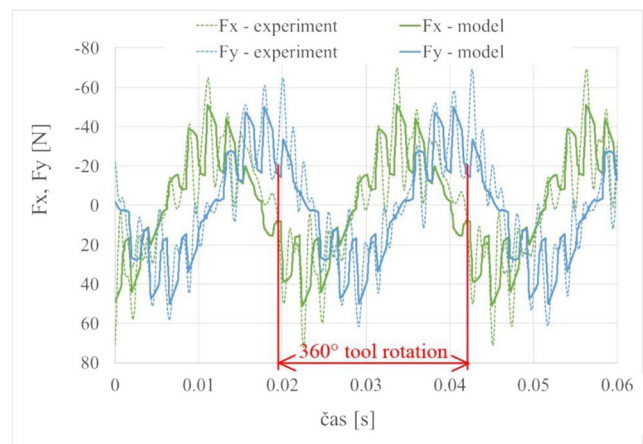
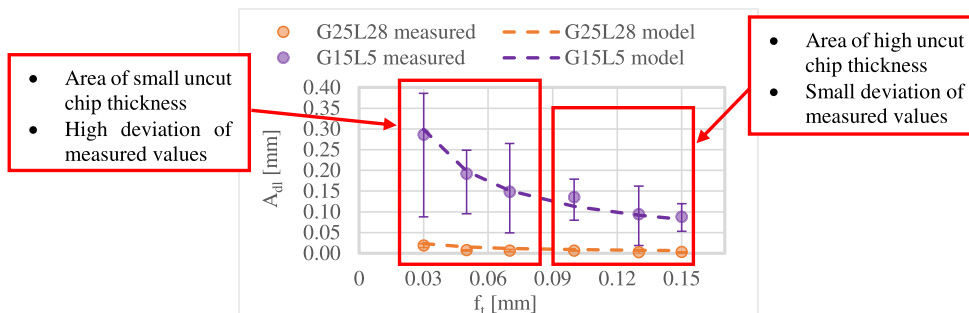


**Fig. 17** Verification of the model for tool G25L15,  $f_i = 0.05$  mm,  $a_e = 3$  mm,  $a_p = 3$  mm,  $v_c = 100$  m/min

**Fig. 18** Dependence of  $A_{dl}$  model on  $f_t$  compared with measured values for tools G25L28 and G15L5



chip thickness, which can be smaller or near the edge radius dimension and material could not be machined properly. This was the reason why the model fits very well but some measured values were relatively outlying as the measurement of G15L5 in Fig. 18 shows.

**5.4 Identification of the temperature model**

The empirical model for temperature of the machined surface was estimated in power form according to the measurement. Coefficients of important factors were also estimated in power function shape on the basis of the least square results. The helix angle was only one statistically significant factor with coefficient  $u_{\theta\lambda}$ .

$$\Theta = C_{\Theta} \cdot v_c^{u_{\Theta}} \cdot \lambda^{u_{\Theta\lambda}}$$

The model of machined surface temperature had a regression coefficient  $R^2 = 0.681$  with values of estimated parameters for the empirical model, as seen in Table 14. The average deviation from real measurements was calculated as less than 7.5%. The maximal deviation was measured as 19% in comparison to the real situation. The deviation of the model from measurements is presented in Fig. 19. The range of measured values was relatively high and this led to the smaller regression coefficient than in the case of force and burr modelling.

**Table 13** Estimation of parameters for  $A_{dl}$  model

Table	Estimate parameter	St. dev.	t-value	p value
$C_{A_{dl}}$	2.724	1.015	2.684	0.011436
$u_A$	-0.806	0.048	-16.845	0.000000
$u_{A\lambda}$	-1.135	0.067	-16.844	0.000000
$u_{A\gamma}$	-1.185	0.114	-10.421	0.000000

**6 Discussion**

This paper focuses on the effects of temperature of the machined surface, cutting forces and average delamination length during C/PPS machining.

**Cutting forces** The measured cutting force values showed the dominant influence of axial depth of cut according to main effect plot but the  $f_t$  had the steepest guideline of dependence  $F_a$  on control factor. It was found that the active cutting force  $F_a$  increased with increasing feed per tooth  $f_t$ , radial depth of cut  $a_e$  and axial depth of cut  $a_p$ . Only if cutting condition  $v_c$  was increased, there was a decrease in  $F_a$  observed. It was discovered that the inflexion point of  $F_a$  was for helix angle  $\lambda_s$  of 15°. The reason of higher cutting force for the higher helix angle would be reduced chip evacuation from the double-helix tool that could clog it up. Therefore, setting the helix angle 15° and employing a higher cutting speed between 500 and 600 m/min are recommended for cutting force minimisation. In addition, the cutting speed could be limited by adjusting the cutting temperature only.

**Cutting temperature** The method for measurement of machined surface temperature based on semi-artificial thermocouple is presented. This method makes use of the electric conductivity in the carbon fibres. The main advantage of this method is the possibility to measure workpiece surface temperature during the cutting process. Utilising the Ni–Cr wire gives good thermoelectric sensitivity of 37.6 °C/mV. However, the method has limited robustness due to high sensitivity of the experiment setup. The Ni–Cr measurement wires should be applied to the coupon very carefully. The only

**Table 14** Estimation of parameters for  $\Theta$  model

Table	Estimate parameter	St. dev.	t-value	p value
$C_{\Theta}$	48.292	8.9689	5.384	0.000011
$u_{\Theta}$	0.191	0.0310	6.152	0.000001
$u_{\Theta\lambda}$	-0.096	0.0226	-4.272	0.000215

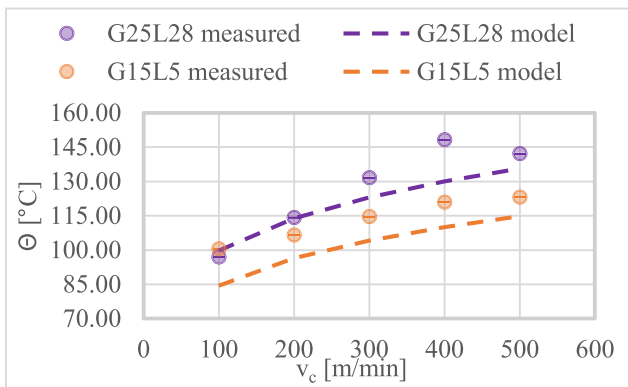


**Fig. 19** Dependence of predicted  $\Theta$  on  $v_c$  compared with measured values for tools G25L28 and G15L5

significant control factor on temperature was cutting speed  $v_c$ . The rake angle value does not have any significant influence on the workpiece surface temperature. During all experiments, the workpiece surface temperature was at maximum 159 °C. It is higher than the C/PPS glass transition temperature, but still far under the 258 °C melting point of the PPS matrix. Since there is a power function dependence with a decreasing temperature gradient (see Fig. 19), there exist potential productivity increases due to an increase in cutting speed. The key constraint is that the workpiece geometry should enable efficient heat evacuation and increasing radial depth of cut (e.g. during inner corner trimming) should be avoided.

**Delamination (burr)** Only type II and type III delamination were observed after machining of C/PPS. It means that only uncut matrix and fibres appear. An upgraded method of delamination measurement promising a high confidence allowed us to measure dependence average delamination length  $A_{dl}$ —feed per tooth  $f_t$ . Delamination was decreased with an increase in feed per tooth. The reason is higher uncut chip thickness could be better cut out. The cutting speed showed a statistically insignificant influence on delamination. When  $a_p$  was increased,  $A_{dl}$  was reduced, as well as for an increased  $f_t$  and increased  $v_c$ . Contrarily, the higher  $a_e$  was, the higher  $A_{dl}$  was. The most suitable variant of cutting geometry for burr reduction was high value of rake angle and value of high helix angle.

## 7 Conclusion

This paper described the influence of cutting conditions and cutting tool geometry on cutting forces, burr and cutting temperature during edge trimming of C/PPS plates. A set of experiments was conducted. The experimental data were used for developing models of cutting forces, burr size and machined surface temperature.

An investigation into cutting conditions was made and the most important cutting condition factors and cutting geometry

were found for cutting forces, surface temperature and average delamination length. An improved geometrical model of the cutting force was presented. The model includes an overlap parameter  $k$ , which increases the accuracy of the model. The average deviation between the cutting force model and measured values was 4%.

The most suitable method for measuring surface temperature was determined and tested with the diamond-based cutting tool. The cutting speed has the greatest influence on workpiece surface temperature. In the next step, a workpiece surface temperature model was developed utilising the experimental data. The model showed a safe temperature level (under PPS melting point) within cutting speeds up to 600 m/min. The average deviation for the workpiece surface temperature model was 7.5%.

The method of delamination measurement was improved for random spatial orientation of burrs. A real average length of burr was measured. Subsequently, the model for delamination was developed although the measured data had a high level of deviation.

All of these models could be used for complex evaluation of cutting conditions and cutting tool geometry during edge trimming of C/PPS plates using cemented carbide tools.

**Funding information** Authors acknowledge support from the EU Operational Programme Research, Development and Education, and from the Center of Advanced Aerospace Technology (CZ.02.1.01/0.0/0.0/16\_019/0000826), Faculty of Mechanical Engineering, Czech Technical University in Prague.

**Open Access** This article is distributed under the terms of the Creative Commons Attribution 4.0 International License (<http://creativecommons.org/licenses/by/4.0/>), which permits unrestricted use, distribution, and reproduction in any medium, provided you give appropriate credit to the original author(s) and the source, provide a link to the Creative Commons license, and indicate if changes were made.

**Publisher's Note** Springer Nature remains neutral with regard to jurisdictional claims in published maps and institutional affiliations.

## References

- Harris B (1999) Engineering Composite Materials. The Institute of Metals, London, p 124
- Puw HY, Hocheng H (1993) Machinability test of carbon fiber-reinforced plastics in milling. Mater Manuf Process 8(6):717–729
- Puw HY, Hocheng H (1993) Machinability of Fiber-Reinforced Thermoplastic in Drilling. J Eng Mater Technol 115:146–149
- Sheikh-Ahmad JY (2009) Machining of polymer composites. Springer Science + Business Media, New York. e-ISBN 978-0-387-68619-6
- Davim PJ (2010) Machining composite materials. ISTE Ltd, London p. 261
- Colligan K, Ramulu M (1991) Delamination in surface plies of graphite/epoxy caused by the edge trimming process.

- Washington: PED-CP.49/MD-Vol.27. Processing and Manufacturing of Composite Materials - ASME
7. Davim PJ, Reis P (2005) Damage and dimensional precision on milling carbon fiber-reinforced plastics using design experiment. *J Mater Process Technol* 160:160–167
  8. Davim PJ, Reis P, Antonio CC (2004) A study on milling of glass fiber reinforced plastics manufactured by hand-lay up using statistical analysis (ANOVA). Elsevier, Porto. *Compos Struct* 64:493–500
  9. Jenarthanan M, Naresh N (2015) Process parameters optimization on machining force and delamination factor in milling of GFRP composite using gray relational analysis. *Indian J Eng Mater Sci* 22:313–320
  10. Szvajka K, Trzepieciński T (2016) Effect of tool material on tool wear and delamination during machining of particleboard. *J Wood Sci* 62:305–315
  11. Praveen R, Perumal AE (2010) Taguchi Analysis of surface roughness and delamination associated with various cemented carbide K10 end mills in milling of GFRP. *J Eng Sci Technol* 3:58–64
  12. Hintze W, Hartmann D, Schütte C (2011) Occurrence and propagation of delamination during the machining of carbon fibre reinforced plastics (CFRPs) – An experimental study. *Compos Sci Technol* 71:1719–1726
  13. Sheikh-Ahmad JY, Dhuttargaon M, Cheraghi H (2017) New tool life criterion for delamination free milling of CFRP. *Int J Adv Manuf Technol* 92:2131. <https://doi.org/10.1007/s00170-017-0240-2>
  14. Jenarthanan MP, Nishanth G, Bharatwaj R (2016) Optimization of machining parameters in end milling of GFRP composites based on the Taguchi method with fuzzy logics. *Int J Knowl-based Intell Eng Syst* 20:123–134. <https://doi.org/10.3233/KES-160338>
  15. Sheikh-Ahmad JY, Urban N, Cherghi H (2012) Machining damage in edge trimming of CFRP. *Mater Manuf Process* 27:802–808
  16. Davies M, Ueda T, M'Saoubi R, Mullany B, Cooke AL (2007) On the measurement of temperature in material removal processes. *Ann CIRP* 56:581–604
  17. Kerrigan K, Thil J, Hewison R (2012) An Integrated Telemetric thermocouple sensor for process monitoring of CFRP milling operations. v 5th CIRP Conference on High Performance Cutting 2012
  18. Kerrigan K, O'Donnell EG (2013) Temperature measurement in CFRP milling using a wireless tool-integrated process monitoring sensor. *Int J Autom Technol* 7:742–750
  19. Jia Z, Fu R, Quan B, He C (2016) Temperature effects in end milling carbon fiber reinforced polymer composites. *Polym Compos* 39:437–447. <https://doi.org/10.1002/pc.23954>
  20. Rahman M, Ramakrishnan S, Thoo HC (1999) Machinability study of carbon/PEEK composites. *Mach Sci Technol* 3(1):49–59
  21. Yoshiro T, Ogawa T, Sasahara H (2013) Temperature measurement of cutting tool and machined surface layer in milling of CFRP. *Int J Mach Tools Manuf* 70:63–69. <https://doi.org/10.1016/j.ijmachtools.2013.03.009>
  22. Wang H, Sun J, Li J, Lu L, Li N (2016) Evaluation of cutting force and cutting temperature in milling carbon fiber-reinforced polymer composites. *Int J Adv Manuf Technol* 1517–1525
  23. Puw HY, Hocheng H (1993) Milling force prediction for fiber reinforced thermoplastics. Winter annual meeting, Machining of advanced composites. LA, ASME, New Orleans. PUBLICATIONS-PED 66:73–88. ISBN:079181033X
  24. Kalla D, Sheikh-Ahmad JY, Twomey J (2010) Prediction of cutting forces in helical end milling fiber reinforced polymers. *Int J Mach Tool Manu* 50:882–891
  25. Karpat Y, Bhtiyar O, Deger B (2012) Milling force modelling of multidirectional carbon fiber reinforced polymer laminates. 5th CIRP Conference on High Performance Cutting 2012
  26. Karpat Y, Polat N (2013) Mechanistic force modeling for milling of carbon fiber reinforced polymers with double helix tools. *CIRP Ann Manuf Technol* 62:95–98
  27. König W, Wulf P, Graß P, Willerscheid H (1985) Machining of fibre reinforced plastics. *CIRP Ann Manuf Technol* 34:537–548
  28. Chatelain J-F, Zaghbani I (2012) A comparison of special helical cutter geometries based on cutting forces for the trimming of CFRP laminates. *Int J Mech* 6:51–59
  29. Chen Y, Fu Y, Su H, Han S (2016) Influence of mill geometry on cutting force and surface morphology of multidirectional CFRP. The 19th international conference on composite materials, Paris
  30. Masek P, Zeman P, Kolar P (2013) Development of cutting tool for composites with thermoplastic matrix. *MM (Modern Machinery) Sci J* 422–427. [https://doi.org/10.17973/MMSJ.2013\\_10\\_201312](https://doi.org/10.17973/MMSJ.2013_10_201312)
  31. Kolar P, Masek P, Zeman P (2014) Milling tools for cutting of fiber-reinforced plastic. *J Mach Eng* 14(2)
  32. Saglam H, Yaldiz S, Unsacar F (2007) The effect of tool geometry and cutting speed on main cutting force and tool tip temperature. *Mater Des* 28:101–111